Scientific Reports

https://doi.org/10.1038/s41598-025-34851-1

Article in Press

Equilibrium modelling and kinetic studies on adsorption of cadmium from lake water by a magnetic covalent organic framework

Received: 31 October 2025

Accepted: 31 December 2025

Published online: 07 January 2026

Cite this article as: Öztürk Er E., Gürsoy S. & Bakırdere S. Equilibrium modelling and kinetic studies on adsorption of cadmium from lake water by a magnetic covalent organic framework. *Sci Rep* (2026). https://doi.org/10.1038/s41598-025-34851-1

Elif Öztürk Er, Selim Gürsoy & Sezgin Bakırdere

We are providing an unedited version of this manuscript to give early access to its findings. Before final publication, the manuscript will undergo further editing. Please note there may be errors present which affect the content, and all legal disclaimers apply.

If this paper is publishing under a Transparent Peer Review model then Peer Review reports will publish with the final article.

ARTICLE IN PRESS

© The Author(s) 2026. **Open Access** This article is licensed under a Creative Commons Attribution-NonCommercial-NoDerivatives 4.0 International License, which permits any non-commercial use, sharing, distribution and reproduction in any medium or format, as long as you give appropriate credit to the original author(s) and the source, provide a link to the Creative Commons licence, and indicate if you modified the licensed material. You do not have permission under this licence to share adapted material derived from this article or parts of it. The images or other third party material in this article are included in the article's Creative Commons licence, unless indicated otherwise in a credit line to the material. If material is not included in the article's Creative Commons licence and your intended use is not permitted by statutory regulation or exceeds the permitted use, you will need to obtain permission directly from the copyright holder. To view a copy of this licence, visit http://creativecommons.org/licenses/by-nc-nd/4.0/.

ARTICLE IN PRESS

Equilibrium modelling and kinetic studies on adsorption of cadmium from lake water by a magnetic covalent organic framework

Elif Öztürk Er[1,2*], Selim Gürsoy[3,4], Sezgin Bakırdere[5,6*]

[1]*İstanbul Technical University, Department of Chemical Engineering, 34469 İstanbul, Türkiye*
[2]*İstanbul Technical University, Polar Research Center, 34469 İstanbul, Türkiye*
[3]*Deparment of Analytical Chemistry, School of Pharmacy, İstanbul Medipol University, 34810, Türkiye*
[4]*Yıldız Technical University, Department of Bioengineering, 34220 İstanbul, Türkiye*
[5]*Yıldız Technical University, Department of Chemistry, 34349 İstanbul, Türkiye*
[6]*Turkish Academy of Sciences (TÜBA), Vedat Dalokay Street, No: 112, 06670, Çankaya, 06690, Ankara, Türkiye*

***Corresponding Authors:** Elif Öztürk Er, ozturkeliff@gmail.com, Sezgin Bakırdere, bsezgin23@yahoo.com

Abstract

Predictive, field-relevant descriptions of cadmium attenuation remain essential for safeguarding freshwater systems. This study evaluates a magnetically retrievable covalent organic framework (COF@Fe_3O_4) sorbent for Cd^{2+} removal from lake water, integrating characterization, equilibrium modelling, and kinetics. The composite was characterized by FT-IR, XRD, and SEM, and its pHpzc was determined. Batch tests were conducted over a pH range of 5.0-9.0, varying contact times, and initial Cd^{2+} concentrations of 20-100 mg L^{-1}. High percent removals were achieved under mildly alkaline conditions, with residual Cd close to the detection limit at pH 9.0 and about 98% removal at the operative dose using simple magnetic handling. Equilibrium behavior was analyzed with parallel nonlinear and linear treatments using consistent error functions. Langmuir provided the best description, yielding q_{max} = 86.99 mg g^{-1} with K_L = 0.0318 L mg^{-1} in nonlinear fitting and q_{max} = 93.67 mg g^{-1} with K_L = 0.0281 L mg^{-1} from the linear form, indicating monolayer uptake on a finite set of sites. Toth also fit well and reflected mild site-energy heterogeneity. Time-dependent uptake for 100 mg L^{-1} Cd^{2+} was the most consistent with a pseudo-second-order model, and intraparticle diffusion analysis gave a positive intercept, indicating a diffusion contribution that is not the sole rate-limiting step. Reusability and structural stability of the material was verified by magnetic recovery with water-only rinsing, maintaining performance across cycles. Overall, the combined characterization, isotherm, and kinetic evidence together with high removals supported COF@Fe_3O_4 as a practical, magnetically separable platform for Cd^{2+} treatment in lake water.

ARTICLE IN PRESS

Key Words: Adsorption; cadmium, lake water, hybrid materials, nonlinear regression.

1. INTRODUCTION

Aquatic contamination remains a persistent concern across surface and groundwater resources. Discharges from mining, electroplating, battery manufacturing, fertilizers, and municipal effluents introduce metal ions that do not undergo biodegradation and can remain mobile under common water chemistry [1,2]. Cadmium is notable for its solubility over much of the environmental pH range and for its tendency to enter aquatic food webs, which sustains exposure risks and underpins stringent regulatory limits (e.g., 3 μg L^{-1} in drinking water as recommended by the WHO) [1,3,4]. In lake water, speciation into hydroxo and carbonate complexes and complexation by natural organic matter (NOM) complicate both removal and quantification; ionic strength and competing cations can vary by season and site [5]. Human exposure occurs primarily through drinking water and diet (notably fish and shellfish) as Cd accumulates in biota and can biomagnify. Chronic Cd exposure is associated with renal dysfunction, bone diseases, and elevated cancer risk [6–8]. These factors motivate removal strategies that remain effective in complex natural waters.

Conventional removal technologies are available but face matrix-dependent constraints. Precipitation and coagulation generate sludge and often struggle near the low microgram per liter (μg L^{-1}) levels. Ion exchange competes poorly against major cations and requires brine management [9–11]. Membrane processes achieve high rejections but are capital intensive and susceptible to fouling by natural organic and inorganic matter [10]. In full-scale treatment plants, these and other sorption-based operations are most commonly implemented in fixed-bed configurations, where granular or pelletized adsorbents are packed in columns operated under continuous flow. For newly developed sorbents, however, batch studies in realistic matrices remain an essential first step to establish intrinsic uptake capacity, pH dependence and kinetic behavior before rational column design and scale-up can be undertaken [12]. Nonetheless, a recurring limitation across these methods is reliance on bulk removal metrics that can mask residual Cd in the dissolved and colloidal fractions of lake water, and efficiencies may appear complete while trace levels persist below routine monitoring ranges. Demonstrating reliable performance therefore requires determinations targeted at the dissolved fraction, size-aware sampling, and calibration that tolerates variability in ionic strength and natural organic matter, with method detection limits aligned to regulatory thresholds [13]. In more complex effluents such as municipal or industrial wastewaters, the coexistence of diverse inorganic ions and organic ligands can further influence Cd^{2+}

ARTICLE IN PRESS

speciation and competitive uptake, and recent studies have highlighted the importance of evaluating adsorbents under such ion-rich conditions when considering wastewater applications [14].

Adsorption is attractive because it is operationally simple, scalable, and amenable to regeneration when the sorbent surface chemistry is matched to the target pollutant, enabling verification of performance at μg L^{-1} in lake water and avoiding overestimation from bulk metrics that can overlook persistent dissolved Cd [15]. Covalent organic frameworks (COFs) offer a programmable route to such sorbents. These crystalline porous polymers provide high surface areas, ordered channels, and functional groups positioned with monomer-level precision [16]. Most COF applications have focused on organic pollutants where π interactions and hydrogen bonding dominate. In contrast, fewer studies have targeted inorganic ions even though COFs can host dense arrays of donor atoms and ion-interacting motifs [17,18]. For metals, adsorption efficacy depends on the availability and geometry of donor sites, hydrolytic stability of the framework, and fast mass transfer through open pores [19,20]. COF structures in the literature utilized for metal removal displays complementary strengths and limitations. For example, beta-ketoenamine COFs are known to be highly stable in water but rely primarily on oxygen donors and often need tighter pH control to match uptake for borderline or soft cations such as Cd^{2+} [21–23]. Sulfurated or ionic COFs can display very high capacities in simple media, yet multi-step or long syntheses and loss of selectivity in the presence of competing anions and dissolved organics can limit use in natural waters [24,25]. Macroscopically immobilized COFs in foams, beads, or aerogels simplify handling and recovery but tend to reduce accessible surface area and introduce intraparticle diffusion barriers that slow equilibration [26–28].

The melamine-terephthalaldehyde imine COF addresses these points from the molecular level upward. Melamine contributes a triazine core with three primary amines; after Schiff-base condensation the framework presents a high density of Lewis-basic nitrogen (imine and ring N) arranged periodically along accessible channels [29]. Terephthalaldehyde provides rigid para-phenylene spacers that help maintain planarity and resist collapse in water, sustaining open, diffusion-efficient pores [30–32]. At circumneutral pH typical of lakes, the basicity and geometry of imine/triazine nitrogen favour inner-sphere coordination of Cd^{2+} while mitigating proton competition; tuning the surface charge near the pH_{pzc} further supports electrostatic contributions without relying on high ionic strength [33,34]. Incorporation of Fe_3O_4 adds benefits beyond magnetic recovery. Dispersed iron-oxide domains introduce surface Fe-OH groups

ARTICLE IN PRESS

that complement the COF's nitrogen donors to create mixed O/N binding environments; the oxide phase can also suppress COF restacking, preserve mesoporosity, and improve mechanical integrity during mixing and regeneration. Magnetism then enables rapid, loss-free phase separation without external forces [35–37]. Therefore, the COF incorporated with Fe_3O_4 was preferred to remove Cd^{2+} from lake waters in order to protect aquatic environments.

This study evaluates removal performance of Cd^{2+} by COF@Fe_3O_4 with attention to adsorption mechanisms at imine/triazine-N and Fe-OH sites together with electrostatic contributions under natural water chemistry. Equilibrium is analyzed using both linear and nonlinear isotherm models to describe site heterogeneity and capacity, with both forms included to enable accurate parameter estimation while maintaining comparability with prior adsorption studies that commonly report linearized constants. Kinetics are evaluated to distinguish external mass transfer from chemisorption and intraparticle diffusion regimes. In parallel, analytical figures of merit (linearity, detection limit, precision, spike recoveries, and potential interferences) are assessed to demonstrate suitability for monitoring near regulatory thresholds. Results are discussed in the context of representative COF and magnetic-hybrid adsorbents to clarify where the melamine-terephthalaldehyde COF@Fe_3O_4 offers, or is likely to offer, advantages in capacity, rate, reusability, and practical handling.

ARTICLE IN PRESS

2. MATERIALS AND METHODS

2.1.Synthesis of COF@Fe_3O_4 magnetic nanomaterial

COF@Fe_3O_4 was prepared in two stages using a coprecipitation step for the magnetic core followed by a solvothermal imine condensation to deposit the COF shell. In the first stage, $FeCl_3 \cdot 6H_2O$ (8.109 g) and $FeSO_4 \cdot 7H_2O$ (4.170 g) were dissolved in 50 mL of deionized water to maintain the stoichiometric Fe^{3+}/Fe^{2+} ratio of 2:1. The solution was diluted with deionized water to a total volume of 250 mL and heated to 80 °C under vigorous stirring to ensure homogeneous mixing and thermal equilibration. Concentrated aqueous ammonia (30 mL) was then introduced dropwise at 80 °C to generate an alkaline medium, promoting supersaturation and coprecipitation of magnetite. A uniform black suspension formed rapidly and was allowed to age for an additional 2 h at 80 °C to complete nucleation and growth. The precipitated Fe_3O_4 was collected magnetically, washed repeatedly with deionized water and ethanol until neutral pH to remove soluble salts and residual base, and dried at 80 °C for 24 h. The obtained Fe_3O_4 nanoparticles were used directly in the subsequent coating step [38].

ARTICLE IN PRESS

For COF deposition, a solvothermal imine condensation was employed. Dried Fe_3O_4 (0.20 g) was dispersed in DMSO (50 mL) containing melamine (2.0 mmol) and terephthalaldehyde (3.0 mmol) and the mixture was sonicated for 30 min to promote wetting of the oxide surface and intimate contact with the monomers. The resulting homogeneous brown suspension was transferred to an autoclave (Teflon-lined stainless-steel) and heated for 24 h at 180 °C, during which interfacial Schiff-base condensation afforded a conformal COF layer on the magnetic cores. The solid part was recovered magnetically and washed three times with anhydrous methanol, dichloromethane, and tetrahydrofuran to remove unreacted monomers and soluble oligomers. The product (COF@Fe_3O_4) was finally dried under vacuum at 50 °C to constant mass [39].

2.2. Determination of cadmium by FAAS system

Cadmium in influent and effluent fractions from the lake water adsorption studies was determined by flame atomic absorption spectrometry (FAAS; ATI UNICAM 929 AA, UNICAM, England). A Cd hollow-cathode lamp operated at 228.8 nm with a 0.50 nm spectral slit and deuterium background correction; atomization employed an air-acetylene flame adjusted close to stoichiometric conditions. Instrument stability was verified by lamp warm-up, baseline checks, and periodic calibration verification standards.

Matrix-matched calibration was prepared by spiking lake water over 0.100-4.0 mg L^{-1} Cd standards. The calibration was linear ($y = 0.0559\ x + 0.0045$, $R^2 = 0.9991$), where *y* is absorbance and *x* is Cd (mg L^{-1}). Limits of detection and quantification were determined as LOD = 3σ/m and LOQ = 10σ/m, using six replicate measurements of the lowest calibrant in the linear range (σ = standard deviation; *m* = slope); the study-specific LOD/LOQ values derived from these criteria are reported with the calibration summary. Results below the working interval were determined at the LOQ, and responses above the linear range were diluted into range. Each analytical set included procedural blanks and triplicate measurements (n = 3). Cd concentrations in all samples were determined from the calibration relationship found.

2.3.Adsorption experiments on lake water

Adsorption capacity (q_e) and removal efficiency (%RE) were employed as complementary response metrics for one-factor-at-a-time (OFAT) optimization in the lake-water matrix. Although detailed in-situ physicochemical measurements were not conducted in the present study, baseline water quality parameters for Büyükçekmece Lake (İstanbul, Türkiye) have

ARTICLE IN PRESS

been reported previously. Seasonal measurements were performed at four sampling stations, and the physicochemical parameters indicated the natural variability of the lake water matrix across seasons and locations, with water temperatures ranging from 4 to 25 °C, pH values from 6 to 8, and dissolved oxygen from 5 to 12 mg/L. Nutrient levels were generally found to be low. Nitrite, phosphate, and nitrate concentrations were below the detection limits for the most of analysis [40]. Büyükçekmece Lake water was used to evaluate adsorption characteristics of COF@Fe3O4 adsorbent under real surface water conditions.

Stock Cd^{2+} solutions were prepared from $CdSO_4 \cdot 3H_2O$ (98%, Riedel-de-Haën, Germany) in deionized water. For each experiment, 30 mL of a lake-water aliquot was spiked to the target initial concentration (C_0), adjusted to the optimum pH value, and combined with COF@Fe_3O_4. The suspension was agitated on an orbital shaker at ambient temperature for 30 min. The solid was separated magnetically, and the Cd^{2+} concentration in the supernatant (C_e) was measured by FAAS. Experiments were conducted in triplicate.

The adsorption capacity q (mg g^{-1}) was calculated as, Eq. (1):

$$q_e = \frac{(C_0 - C_e)V}{m} \quad (1)$$

and the removal efficiency (%) as Eq. (2):

$$\%RE = 100 * \frac{C_0 - C_e}{C_0} \quad (2)$$

- V - volume of the lake water sample used in each batch adsorption after pH adjustment and spiking to C_0 (L)
- m - mass of the COF@Fe_3O_4 composite added to each batch adsorption (g)
- C_0 - initial Cd^{2+} concentration in the pH-adjusted lake-water aliquot at t = 0, immediately before contact with COF@Fe_3O_4 (mg L^{-1})
- C_e -residual Cd^{2+} concentration in the same aliquot after 30 min contact and magnetic separation, determined by FAAS (mg L^{-1})

2.4.Adsorption isotherms and kinetics

Batch adsorption of Cd^{2+} by COF@Fe_3O_4 in lake water matrix was conducted at optimized conditions at (25 ± 1) °C. Equilibrium studies used initial concentrations of 20-100 mg L^{-1}, and kinetic experiments used 100 mg L^{-1} with contact times of 10-120 min. After magnetic separation, the residual Cd^{2+} concentration in solution was measured and the adsorbed amount at each sampling time (q_t, including q_e at equilibrium) was calculated using Eq. (1). Equilibrium adsorption was analyzed with linearized and nonlinear variants of six isotherm

ARTICLE IN PRESS

models: Langmuir, Freundlich, Sips, Temkin, Dubinin-Radushkevich (DR), and Toth. Kinetic data were fitted in both linearized and nonlinear forms to the pseudo-first-order, pseudo-second-order, and Weber-Morris intraparticle-diffusion models. Both regression approaches were applied to ensure robust nonlinear parameter estimation while also preserving compatibility with earlier adsorption studies that traditionally report linearized constants. Nonlinear estimation employed a trial-and-error iterative scheme in which model parameters were optimized separately with respect to each error criterion (SSE, χ^2, ARE, RMSE, HYBRID), rather than relying solely on least-squares minimization. Model adequacy was then judged using the full set of error metrics, and the reported fits correspond to parameter sets that performed consistently well across these criteria while remaining physically reasonable for both the equilibrium and kinetic data. The full set of linear and nonlinear equation forms, parameter symbols, and units for all isotherm and kinetic models is provided in Table 1 [41–44].

ARTICLE IN PRESS

ARTICLE IN PRESS

Table 1. The list of isotherm and kinetic models, and error functions

Model		Linear Form	Non-Linear Form	Parameters
Adsorption Isotherms				
	Langmuir	$\frac{C_e}{q_e} = \frac{1}{K_L q_{mL}} + \frac{1}{q_{mL}} C_e$	$q_e = \frac{q_{mL} K_L C_e}{1 + K_L C_e}$	q_{mL} and K_L
	Freundlich	$q_e = lnK_F + \frac{1}{n} lnC_e$	$q_e = K_F C_e^{\frac{1}{n}}$	K_F and n
Two parameter models	Temkin	lnC_e lnK_T	$= BlnK_T BlnC_e$ $B = \frac{RT}{b_T}$	$B\ and\ K_T$
	Dubinin-Radushkevich (DR)	$lnq_e = lnq_s - K_{DR}\varepsilon^2$ $\varepsilon = RTln(1 + \frac{1}{C_e})$	$q_e = q_s \exp(-K_{DR}\varepsilon^2)$	$\varepsilon\ and\ K_{DR}$
Three parameter models	Sips	$\ln(\frac{q_e}{q_{m-}q_e}) = \beta_S lnC_e - lnK_s$	$q_e = \frac{q_{mL} K_S C_e^{\beta_S}}{1 + K_S C_e^{\beta_S}}$	q_{mL}, K_S and β_S
	Toth	$\ln(\frac{q_e}{q_{m-}q_e}) = \frac{1}{tn} lnC_e - lnK_{To}$	$q_e = \frac{q_{mL} C_e}{(K_{To} + C_e^{tn})^{\frac{1}{tn}}}$	$q_{mL}\ and\ K_{To}$ and tn
Adsorption Kinetics				
Empirical models	Pseudo-first-order kinetics	$\ln(q_e - q_t) = lnq_e - k_1 t$	$q_t = q_e(1 - e^{-k_1 t})$	q_e and k_1
	Pseudo-second-order kinetics	$\frac{1}{q_t} = \frac{1}{k_2 q_e^2}(\frac{1}{t}) + \frac{1}{q_e}$	$q_t = \frac{q_e^2 k_2 t}{1 + q_e k_2 t}$	q_e and k_2
Internal diffusion model	Weber and Morris (W-M) kinetics model	$q_t = k_{wm} t^{0.5} + C$	-	k_{wm} and C
Error functions				

$$R^2 = \frac{\sum_{i=1}^{n}(q_{e,exp} - \overline{q_{e,calc}})^2}{\sum_{i=1}^{n}(q_{e,exp} - \overline{q_{e,calc}})^2 + \sum_{i=1}^{n}(q_{e,exp} - q_{e,calc})^2}$$

$$ARE = \frac{100}{n}\sum_{i=1}^{n}\left|\frac{q_{e,exp} - q_{e,calc}}{q_{e,exp}}\right|$$

$$Chi - square\ (\chi^2) = \sum_{i=1}^{n}\frac{(q_{e,exp} - q_{e,calc})^2}{q_{e,calc}}$$

$$RMSE = \sqrt{\frac{1}{n-p}\sum_{i=1}^{n}(q_{e,exp} - q_{e,calc})^2}$$

ARTICLE IN PRESS

ARTICLE IN PRESS

$$HYBRID = \frac{100}{n-p}\sum_{i=1}^{n}\frac{\left(q_{e,exp}-q_{e,calc}\right)^2}{q_{e,exp}}$$

q_m is the maximum adsorption capacity (mg g^{-1}); q_e is the amount of Cd^{2+} adsorbed at equilibrium (mg g^{-1}); K_L is the Langmuir constant (L mg^{-1}); K_F is the Freundlich constant; n is the Freundlich heterogeneity parameter (dimensionless); $B = \frac{RT}{b_T}$ is the Temkin constant (J mol^{-1}); K_T is the Temkin equilibrium binding constant (L mg^{-1}); q_s is the theoretical saturation capacity in the Dubinin–Radushkevich model (mg g^{-1}); K_{DR} is the Dubinin–Radushkevich constant (mol^2 kJ^{-2}); $\varepsilon = RTln\left(1+\frac{1}{c_e}\right)$ is the Polanyi potential (kJ mol^{-1}); K_S and β_S are the Sips isotherm constant (L mg^{-1}) and heterogeneity exponent (dimensionless); K_{To} and tn are the Toth isotherm constant (L mg^{-1}) and exponent (dimensionless). R is the universal gas constant (8.314 J mol^{-1} K^{-1}). k_1 is the pseudo-first-order rate constant (min^{-1}); k_2 is the pseudo-second-order rate constant (g mg^{-1} min^{-1}); q_t is the adsorption amount at time t (mg g^{-1}); k_{wm} is the intraparticle diffusion rate constant in the Weber–Morris model (mg g^{-1} min$^{-1/2}$); C is the boundary-layer thickness parameter (mg g^{-1}).

2.5. Fourier-transform infrared spectroscopy (FT-IR)

IR spectra of the COF/Fe_3O_4 material were recorded on a PerkinElmer Spectrum Two FT-IR equipped with a Universal ATR accessory (diamond, single reflection; 75 N applied force). Spectra were acquired in the mid-IR region (4000-450 cm^{-1}) at 2 cm^{-1} resolution with 32 co-added scans, using a $LiTaO_3$ detector and KBr beamsplitter; axes were cm^{-1} (x) and %T (y). Data were processed in Spectrum with magnitude phase correction (scan speed 0.2; combined scan direction). The sample was analyzed neat on the ATR diamond.

2.6. X-ray diffraction

Powder XRD patterns of COF@Fe_3O_4 were collected on a Bruker D2 PHASER (2nd Gen) equipped with a Cu Kα tube (λ = 1.54184 Å) and a LYNXEYE XE-T one-dimensional detector, operated in coupled θ-2θ geometry. The generator was set to 30 kV and 10 mA. Scans were acquired in continuous PSD fast mode over 2θ = 10.00-90.00° with a step size of 0.0202° and 0.150 s per step (PSD opening = 2.94°). Samples were gently ground, spread on a low-background Si holder, and measured at ambient conditions (25 ± 1 °C). Phase identification was performed by comparison with reference patterns.

2.7. Scanning electron microscopy: morphological studies

The surface morphology of COF@Fe_3O_4 was examined by scanning electron microscopy (SEM). Micrographs were acquired using a Zeiss EVO LS10 operated in beam mode at an acceleration voltage of 10 kV. Samples were affixed to aluminum stubs with conductive

ARTICLE IN PRESS

carbon tape and sputter-coated with a thin Au-Pd film under argon using a Quorum SC7620 sputter coater to minimize charging. Images were collected from representative regions to assess particle size, surface texture, and agglomeration state.

2.8. Determination of point of zero charge

The point of zero charge (pH_{pzc}) of COF@Fe_3O_4 was determined by the solid-addition method [38]. Briefly, a series of 50 mL Erlenmeyer flasks, each containing 25 mL of 0.10 M KNO_3 (supporting electrolyte, constant ionic strength), were prepared. The initial pH (pH_0) was adjusted from 2.0 to 11 using 0.10 M HCl or 0.10 M NaOH. To each flask, 25 mg of COF@Fe_3O_4 was added; the vessels were immediately capped to minimize atmospheric CO_2 uptake, and the suspensions were equilibrated for 24 h at 25 ± 1 °C on an orbital shaker (150 rpm). After equilibrium, the final pH (pH_f) was measured and ΔpH was calculated as $\Delta pH = pH_0 - pH_f$. A plot of ΔpH versus pH_0 was constructed, and the intersection with ΔpH = 0 was taken as pHpzc. All measurements were performed in triplicate (n = 3); a no-sorbent control confirmed negligible drift in electrolyte pH under identical conditions.

3. RESULTS AND DISCUSSION

3.1. COF@Fe_3O_4 characterization

3.1.1. Infrared analysis: FT-IR

As displayed in Figure 1, the FT-IR spectrum of COF@Fe_3O_4 demonstrates the combined signatures of an imine-linked COF shell and a magnetite core, confirming successful integration. A distinct band at 1538 cm^{-1} corresponds to the C=N stretching of the Schiff-base linkage, while features at 1470 cm^{-1} and 1344 cm^{-1} reflect aromatic skeletal vibrations and C-N stretching typical of the melamine-terephthalaldehyde framework. Additional bands at 1186 and 983 cm^{-1} arise from in-plane C-H and C-N modes of the conjugated imine/aryl backbone. Out-of-plane C-H deformations characteristic of a 1,4-disubstituted benzene ring appear at 863 and 811 cm^{-1}, supporting the presence of para-phenylene linkers. Importantly, there is no detectable carbonyl band near 1690-1720 cm^{-1} from the aldehyde precursor and no distinct primary-amine stretches around 3300-3500 cm^{-1} from melamine, indicating that -CHO and -NH_2 groups were consumed during Schiff-base condensation. The magnetic phase is verified by strong Fe-O lattice vibrations centered at 567 and 447 cm^{-1}, which are characteristic of octahedral and tetrahedral sites in magnetite (Fe_3O_4). Altogether, the emergence of imine and aryl signatures, the disappearance of precursor bands, and the preserved Fe-O modes in Figure

ARTICLE IN PRESS

1 demonstrate formation of an imine-linked COF shell firmly associated with a structurally intact Fe_3O_4 core [39,45–47].

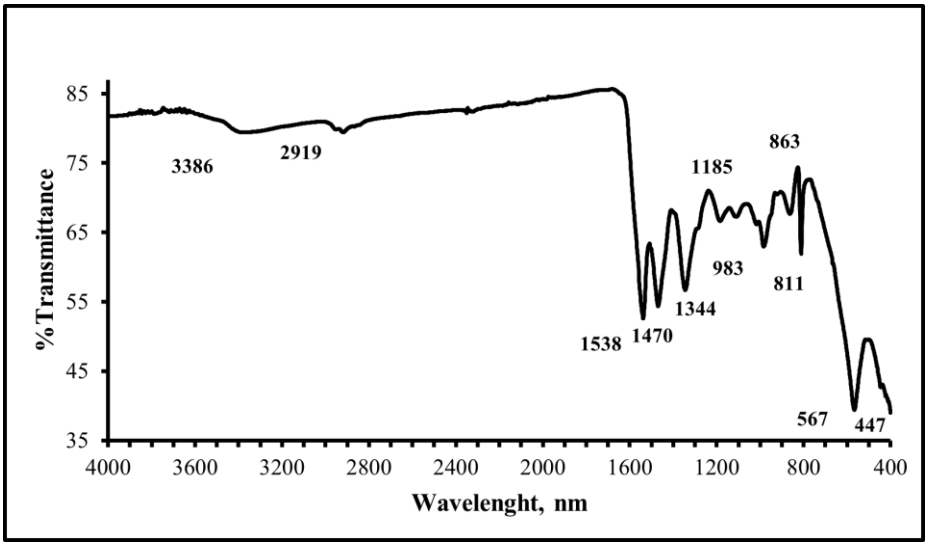


Fig 1. FT-IR spectra of COF@Fe_3O_4 composites.

3.1.2. X-ray diffraction analysis

As shown in Figure 2, the diffraction pattern of COF@Fe_3O_4 matches the reference magnetite card (PDF 01-084-2182) with the characteristic spinel reflections at 2θ = 30.2° (220), 35.5° (311), 43.2° (400), 53.6° (422), 57.1° (511), and 62.7° (440). No additional peaks or peak shifts are observed after COF incorporation, indicating that the Fe_3O_4 lattice remains intact and that the organic shell does not induce phase transformation or oxidation. The minor attenuation in relative intensities and the slightly elevated background at low angles are consistent with a thin, largely amorphous COF layer on the magnetic core rather than separate crystalline by-products. Overall, the XRD data confirm that the crystallographic structure of Fe_3O_4 is preserved in COF@Fe_3O_4 and that the COF deposition proceeds without altering the spinel framework [39].

ARTICLE IN PRESS

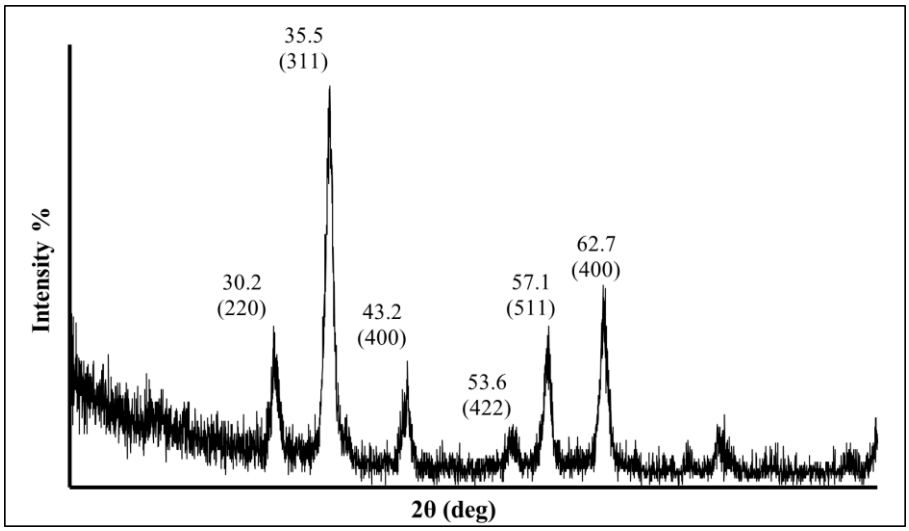


Fig 2. XRD spectra of COF@Fe_3O_4 composites.

3.1.3. Morphological analysis: SEM

As shown in Figure 3, the SEM images indicate loosely aggregated particles that form micron-scale clusters. Within these clusters, higher-magnification areas show a fine speckled texture consistent with nanometer-sized primary particles, although individual boundaries are not clearly resolved at the available image quality. Plate-like or needle-like coarse crystallites are not evident in the fields of view and no large debris is observed. Given these limitations, the images are interpreted qualitatively and the material is described as nanoscale primary domains assembled into secondary agglomerates, a configuration typically associated with high effective surface area and short diffusion paths during adsorption [48,49].

ARTICLE IN PRESS

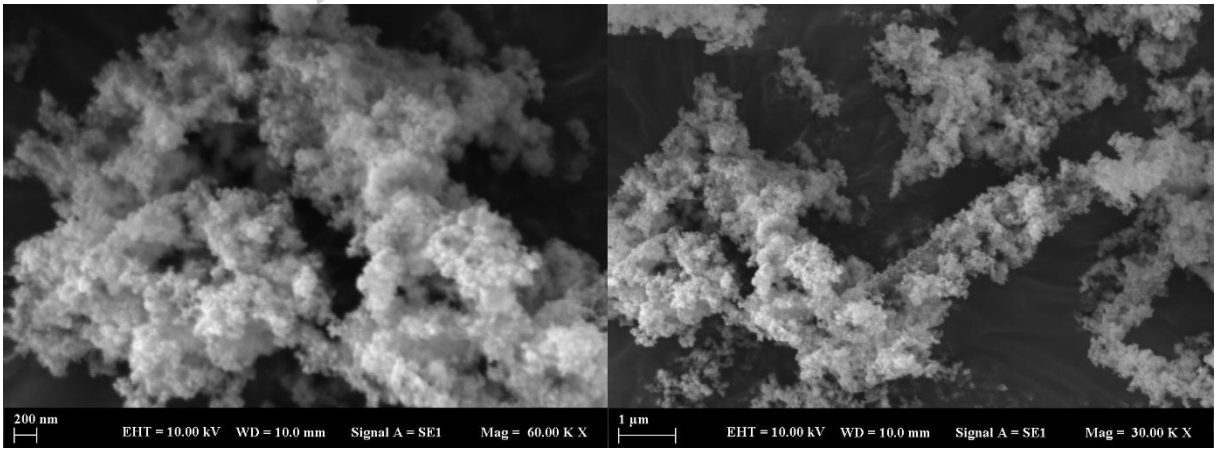


Fig 3. SEM images of COF@Fe_3O_4

3.2. Effect of adsorption parameters

3.2.1. Effect of pH

ARTICLE IN PRESS

One of the key variables governing adsorption-based Cd removal is the pH of the medium, because pH simultaneously controls cadmium speciation and the charge state of the adsorbent [50]. In this study pH 5.0-9.0 was examined, with each target value maintained by suitable buffer solutions and the suspensions allowed to equilibrate before measurement. The solid addition plot of ΔpH versus pH_0 gave a pH_{pzc} of about 4.2 for COF@Fe_3O_4, as shown in Figure 4a, which establishes the electrostatic context for the uptake experiments. Below this point the surface is positively charged and the donor groups identified by FT-IR, namely imine C=N environments, C-N sites from melamine units, and surface -OH on Fe_3O_4, remain largely protonated. Protonation limits coordination by reducing available lone pairs and also introduces electrostatic repulsion against Cd^{2+} so removal is weak at low pH. As pH increases above the pH_{pzc} those same -OH and imine-adjacent nitrogen centres gradually deprotonate, the surface charge shifts negative, and inner sphere complexation together with electrostatic attraction toward Cd^{2+} becomes favored [51–53]. In aqueous solution cadmium is predominantly Cd^{2+} from mildly acidic to near neutral conditions, while minor hydrolyzed forms such as $Cd(OH^+)$ grow in importance as pH rises [1]. These coupled effects lead to the profile in Figure 4b, where removal increases steadily from pH 5 to pH 9 and the response becomes more consistent at higher pH, indicating more stable binding at deprotonated sites. Values above pH 9 were not examined to prevent the major contribution of $Cd(OH)_2$. At the optimized pH 9.0 condition, the residual signal reaches the method LOD, demonstrating near quantitative uptake while staying below the range where precipitation interferes. For these reasons pH 9.0 was selected as the operating pH in subsequent experiments.

ARTICLE IN PRESS

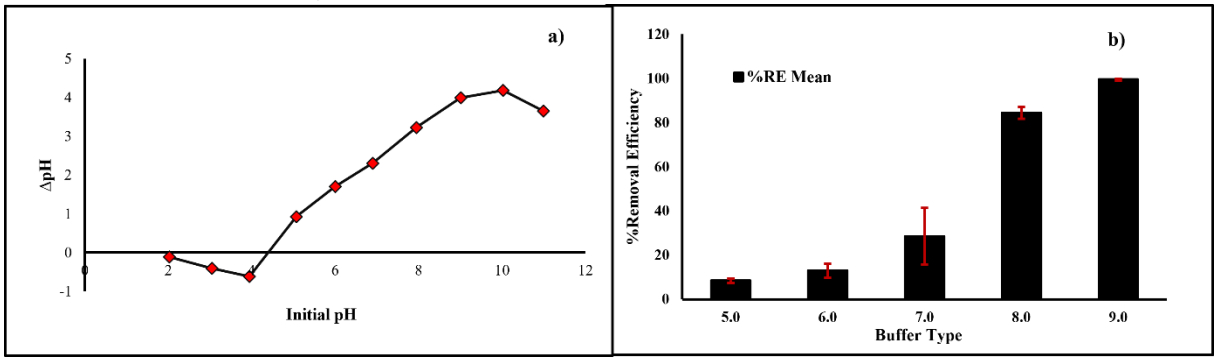


Fig. 4 (**a**) Point of zero charge of COF@Fe_3O_4 nanocomposites and (**b**) optimization of pH of the medium (n = 3) (The constant parameters; 5.0 mg L^{-1} of Cd^{2+} standard solution, 10 mL sample volume, 30 min of mechanical shaker mixing, agitation speed of 250 rpm, 25 mg of adsorbent)

ARTICLE IN PRESS

3.2.2. Effect of nanocomposite amount

The mass of sorbent with a fixed volume at a fixed Cd concentration determines the number of accessible binding sites and the effective solid liquid interfacial area, so it directly governs how quickly and how completely Cd^{2+} is adsorbed from solution [54]. In this study, 10-100 mg of COF@Fe_3O_4 was examined under otherwise identical conditions. As displayed in Figure 5, increasing the dose from 10 mg to 25 mg noticeably raised removal, and a further increase to 50 mg yielded near quantitative uptake with very low residual signal and excellent precision (%RSD about 0.1). Beyond 50 mg, additional gains were minimal and a plateau appeared at 75-100 mg, which is consistent with site saturation at the chosen loading and with crowding effects where particle aggregation and overlap reduce the incremental surface area exposed to solution [55]. The trend agrees with the surface chemistry discussed earlier, where higher sorbent mass introduces more deprotonated -OH and imine-adjacent N donor sites at the working pH, strengthening inner sphere complexation and electrostatic attraction of Cd^{2+} until the dissolved Cd becomes limiting. For the subsequent removal studies covering various initial Cd concentrations, 50 mg was selected as the optimum adsorbent mass.

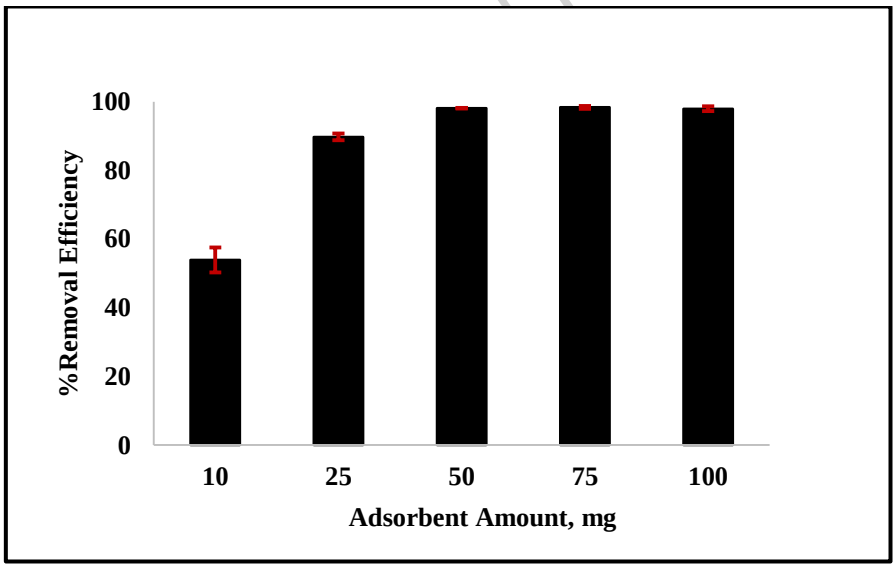


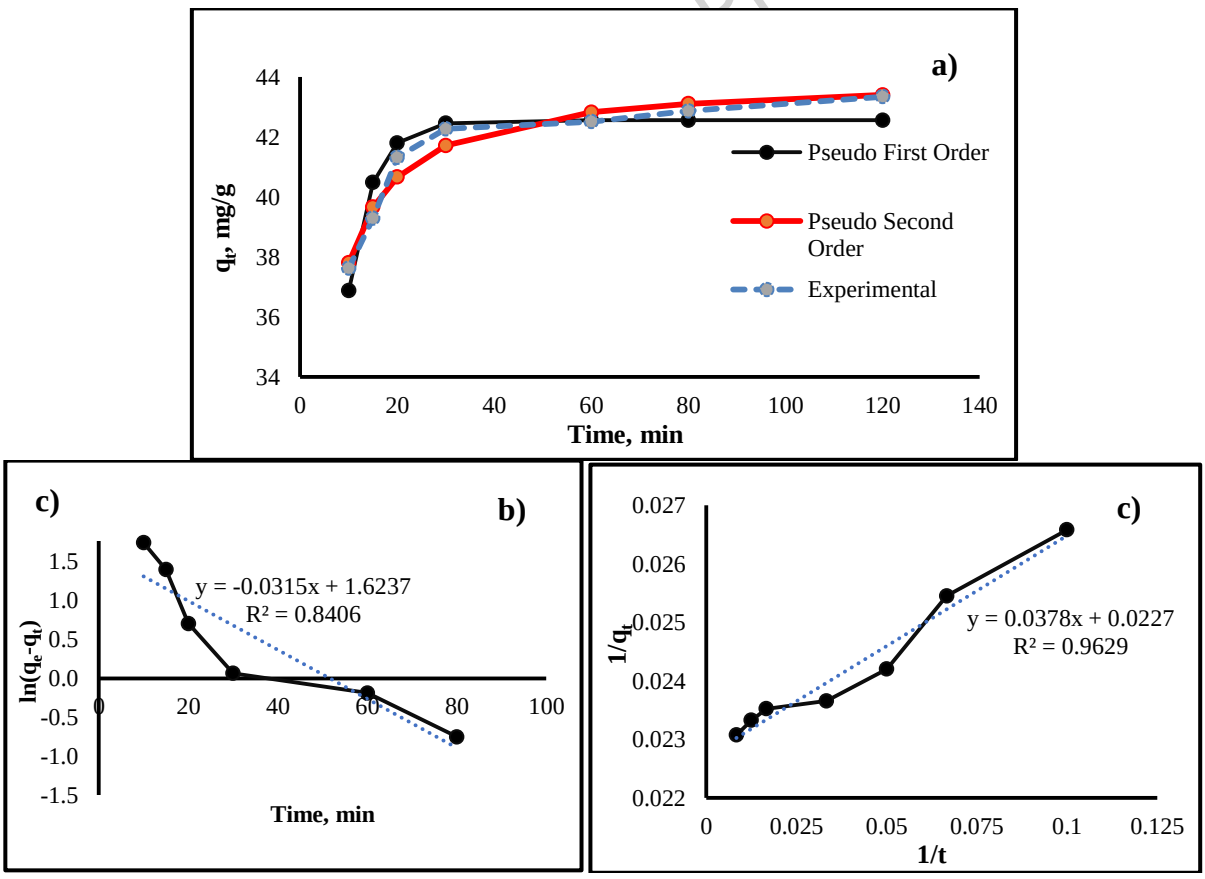
Fig. 5 The effect of adsorbent amount (n = 3) (The constant parameters: 30 mL sample volume, 5.0 mg L^{-1} of Cd^{2+} standard solution, agitation speed of 250 rpm, 30 min of mechanical shaker mixing)

,

3.3. Adsorption kinetics

ARTICLE IN PRESS

The kinetic data of Cd^{2+} (100 mg L^{-1}) removal from lake water were evaluated using nonlinear and linearized versions of the pseudo-first-order (PFO), pseudo-second-order (PSO), and intraparticle diffusion (IPD). The governing equations and error functions are given in Table 1, figure 6 illustrates the plots of both linear and non-linear forms of kinetic models and the kinetic constants with fit statistics are reported in Table 2. As shown in Figure 6, the removal efficiency increased rapidly during the initial contact period and then approached a plateau after approximately 30 minutes, indicating that adsorption equilibrium was effectively reached within this time frame. Beyond 30 minutes, no pronounced improvement in removal efficiency was observed. This behavior demonstrates that a contact time of 30 minutes is sufficient to achieve adsorption equilibrium under the investigated conditions.



ARTICLE IN PRESS

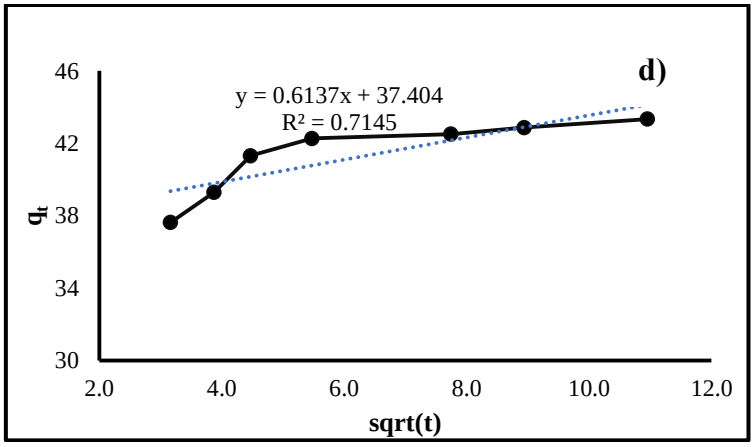


Fig 6. (**a**) Experimental and calculated data which were obtained from non-linear fitting, respectively; (**b-c-d**) linear plots for PFO, PSO and IPD plots, respectively, for the adsorption Cd^{2+} onto $COF@Fe_3O_4$ composites

Table 2. Estimated nonlinear and linear kinetic parameters for adsorption of Cd^{2+} by $COF@Fe_3O_4$ composites.

	Linearized Parameters Values			**Nonlinear Parameters Values**	
PFO parameters	$k_{1\,(min^{-1})}$	0.0315	**PFO parameters**	$k_{1\,(min^{-1})}$	0.2013
	$q_e\ (mg\ g^{-1})$	5.071		$q_e\ (mg\ g^{-1})$	42.55
	R^2	0.8406		R^2	0.8891
	X^2	17.69		X^2	0.0731
	ARE	1.0023		ARE	0.0925
	$RMSE$	7.992		$RMSE$	0.6490
	$HYBRID$	11.53		$HYBRID$	0.0736
PSO parameters	$k_2\ (g\ mg^{-1}\ min^{-1})$	0.0136	**PSO parameters**	$k_2\ (g\ mg^{-1}\ min^{-1})$	0.01389
	$q_e\ (mg\ g^{-1})$	44.03		$q_e\ (mg\ g^{-1})$	43.99
	R^2	0.9629		R^2	0.9597
	X^2	0.0261		X^2	0.0260
	ARE	0.0580		ARE	0.0576
	$RMSE$	0.3923		$RMSE$	0.3909
	$HYBRID$	0.0259		$HYBRID$	0.0258
IPD para	$k_{wm}\ (mg\ g^{-1}\ min^{\frac{-1}{2}})$	0.6137			

ARTICLE IN PRESS

	$C\ mg\ g^{-1}$	37.40
	R^2	0.7145
	X^2	0.1883
	ARE	0.1493
	$RMSE$	1.041
	$HYBRID$	0.1891

The nonlinear PFO model described the initial increase of q_t but underestimated the approach to equilibrium. It returned q_e = 42.55 mg g^{-1} with k_1 = 0.201 min^{-1} and R_2 = 0.889 in the q_t domain, which deviates from the measured equilibrium uptake of about 43-44 mg g^{-1} and is accompanied by error statistics that remain inferior to those of the PSO model. Its linearized version performed considerably worse, producing an implausible q_e of 5.071 mg g^{-1} and a low graphical R^2, indicating that a simple first-order rate expression is unlikely to explain the overall process [56].

In contrast, the PSO model provided a more consistent description of the kinetic data. The nonlinear PSO fit gave q_e = 43.99 mg g^{-1} with k_2 = 0.0139 g mg^{-1} min^{-1} and R^2 = 0.960, closely matching the experimental equilibrium value. The linear PSO expression likewise yielded realistic q_e values and higher correlation coefficients than the corresponding PFO linearization. These results indicate that a PSO-type expression is a suitable empirical descriptor of the rate under the present conditions without, by itself, proving a specific bonding mechanism [57,58].

The IPD model yielded k_{wm} = 0.614 mg g^{-1} $min^{-0.5}$, intercept C = 37.40 mg g^{-1}, and a graphical R^2 of 0.715. The positive intercept indicates that intraparticle diffusion contributes to the overall process but is not the only rate-influencing step, and film diffusion likely affects the early stage [59].

Overall, the combination of higher R^2, lower error-function values (χ^2, ARE, RMSE, HYBRID), and realistic q_e estimates for the PSO model, together with the weaker performance of PFO and the nonzero IPD intercept, indicates that the kinetics are best represented by a PSO-type model with mixed transport influences from film and intraparticle diffusion. This should be regarded as an empirical rate description rather than definitive evidence for a particular adsorption mechanism.

ARTICLE IN PRESS

3.4. Adsorption isotherms

Researchers continue to refine adsorption descriptions because of their industrial relevance. In this work, equilibrium experiments used lake water samples spiked with Cd^{2+} at 20-100 mg L^{-1}, and Fig. 7 (a) shows q_e (mg g^{-1}) versus C_e (mg L^{-1}). The isotherm set comprised Langmuir, Freundlich, Temkin, Sips, Dubinin-Radushkevich (D-R), and Toth. The Langmuir, Freundlich, Temkin, and Dubinin-Radushkevich (D-R) isotherms were evaluated using both nonlinear regression and their corresponding classical linearized forms. The Sips and Toth isotherms were evaluated using nonlinear regression only, and their linearized forms were not considered in the present analysis due to the complexity of their linear forms. The governing equations and error-function definitions (RSS, RMSE, χ^2, ARE, HYBRID, R^2) are given in Table 1, and fitted parameters for both treatments are summarized in Table 3 and Table 4. Toth provides the closest agreement and indicates mild site-energy heterogeneity through its exponent t = 3.7359, which is consistent with a Langmuir-like adsorption behavior at moderate to high C_e. Langmuir quantifies a finite monolayer capacity and an affinity that yields a dimensionless separation factor $0 < RL < 1$ across 20-100 mg L^{-1}; the fitted monolayer capacities were q_m = 86.99 mg g^{-1} (nonlinear) and q_m = 93.67 mg g^{-1} (linear), both exceeding the maximum experimental q_e and indicating that saturation was not reached in this range. Freundlich supports heterogeneity with n = 1.4838, coherent with the Toth result, while Sips gives a heterogeneity index n = 1.3472 that trends toward Langmuir behavior at higher C_e while accommodating dispersion at lower C_e. Temkin yields B = 17.1596, indicating a decrease in adsorption heat with increasing coverage, and nonlinear D-R gives a mean adsorption energy ε = 0.2209 kJ mol^{-1}, placing the process in the physisorption regime and aligning with the affinity implied by the site-based models [60]. Linear results are reported alongside the nonlinear fits in Table 3 and Table 4, and Figure 7(b–c-d) presents linearized plots for the Langmuir, Freundlich and Temkin models, which gave the most consistent linear fits; parameters obtained from the linear plots were back-transformed to the natural response scale (q_e, mg g^{-1}), and the same error functions (RSS, RMSE, χ^2, ARE, HYBRID, R^2) were computed to enable direct comparison with the non-linear models. Overall, the dataset is explained primarily by Toth and Langmuir, while the supporting values from Freundlich (n > 1) and Sips (n close to 1) indicate mild heterogeneity superimposed on predominantly monolayer uptake over 20-100 mg L^{-1}.

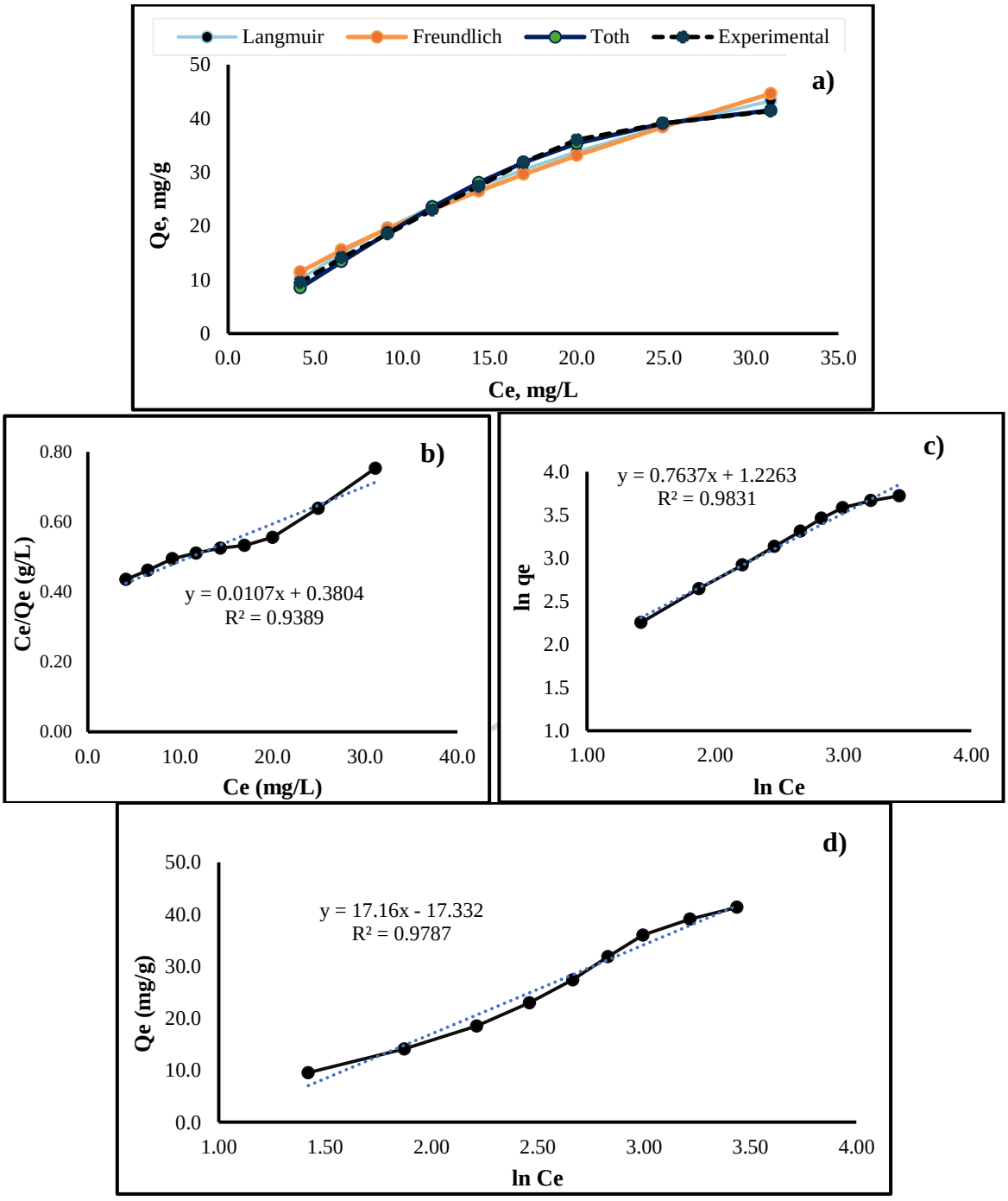


Fig. 7 **(a)** Nonlinear and **(b-c-d)** linear Langmuir, Freundlich and Temkin isotherms, respectively, for the adsorption of Cd^{2+}onto $COF@Fe_3O_4$ composites.

ARTICLE IN PRESS

Table 3. Estimated nonlinear isotherm parameters for adsorption of Cd^{2+} by COF@Fe_3O_4 composites.

Langmuir Parameters		**Freundlich Parameters**	
$q_{mL}\ (mg\ g^{-1})$	86.989	n	1.483
$K_L\ (L\ mg^{-1})$	0.0318	$K_F\ (mg\ g^{-1})(L\ mg^{-1})^{1/n}$	4.393
R^2	0.9868	R^2	0.9684
X^2	0.4587	X^2	1.214
ARE	37.85	ARE	64.43
$RMSE$	13.38	$RMSE$	32.03
$HYBRID$	0.4608	$HYBRID$	1.281
Sips Parameters		**Toth Parameters**	
$q_{mS}\ (mg\ g^{-1})$	59.02	$q_{mT}(mg\ g^{-1})$	43.99
β_S	1.347	t_o	3.735
$K_S(L\ mg^{-1})$	0.0642	$K_T(L\ mg^{-1})$	0.046
R^2	0.9929	R^2	0.9972
X^2	0.3287	X^2	0.1958
ARE	32.88	ARE	23.56
$RMSE$	7.186	$RMSE$	2.766
$HYBRID$	0.3169	$HYBRID$	0.1827
Temkin		**Dubinin-Radushkevich (D-R)**	
$K_T(L\ mg^{-1})$	0.3642	$q_{mDR}\ (mg\ g^{-1})$	40.65
$b_t(J\ mol^{-1})$	17.16	$\beta(mol^2\ kJ^{-2})$	1.0251×10^{-5}
R^2	0.9787	R^2	0.8932
X^2	1.467	X^2	27.67
ARE	65.86	ARE	157.02
$RMSE$	21.61	$RMSE$	108.3
$HYBRID$	1.279	$HYBRID$	7.953

ARTICLE IN PRESS

ARTICLE IN PRESS

Table 4. Estimated linear isotherm parameters for adsorption of Cd^{2+} by COF@Fe_3O_4 composites.

Langmuir Parameters		**Freundlich Parameters**	
$q_{mL}(mg\ g^{-1})$	93.66	n	1.3093
$K_L\ (L\ mg^{-1})$	0.0280	$K_F\ (mg\ g^{-1})(L\ mg^{-1})^{1/n}$	3.4087
R^2	0.9389	R^2	0.9831
X^2	0.4257	X^2	1.1685
ARE	29.66	ARE	44.035
$RMSE$	14.61	$RMSE$	46.68
$HYBRID$	0.4188	$HYBRID$	1.2420
Temkin		**Dubinin-Radushkevich (D-R)**	
$K_T(L\ mg^{-1})$	0.3642	$q_{mDR}(mg\ g^{-1})$	33.91
$b_t(J\ mol^{-1})$	17.15	$\beta(mol^2\ kJ^{-2})$	5.056×10^{-6}
R^2	0.9787	R^2	0.8441
X^2	1.467	X^2	7.7025
ARE	65.86	ARE	156.9
$RMSE$	21.61	$RMSE$	214.7
$HYBRID$	1.279	$HYBRID$	7.708

ARTICLE IN PRESS

3.5.Possible adsorption mechanisms

As displayed in Figure 8, cadmium uptake by COF@Fe_3O_4 may proceed through a coupled pathway in which electrostatic interactions guide ions to the interface, physical sorption concentrates them on accessible surfaces, and chemical sorption provides stronger attachment at reactive centers. A pH_{pzc} of about 4.2 frames the surface environment across the studied pH 5.0-9.0 range. Below this point the surface is expected to be positively charged and donor groups largely protonated, so only relatively weak, nonspecific interactions such as electrostatic attraction and outer-sphere coordination are expected to occur. With increasing pH, -OH groups on magnetite and nitrogen sites adjacent to the imine C=N linkages in the COF shell could become progressively deprotonated, shifting the surface charge negative and encouraging approach of Cd^{2+}, consistent with the rise in removal efficiency observed at higher pH values (Figure 4b). This shift is consistent with the observed rise in removal toward alkaline conditions [61,62].

ARTICLE IN PRESS

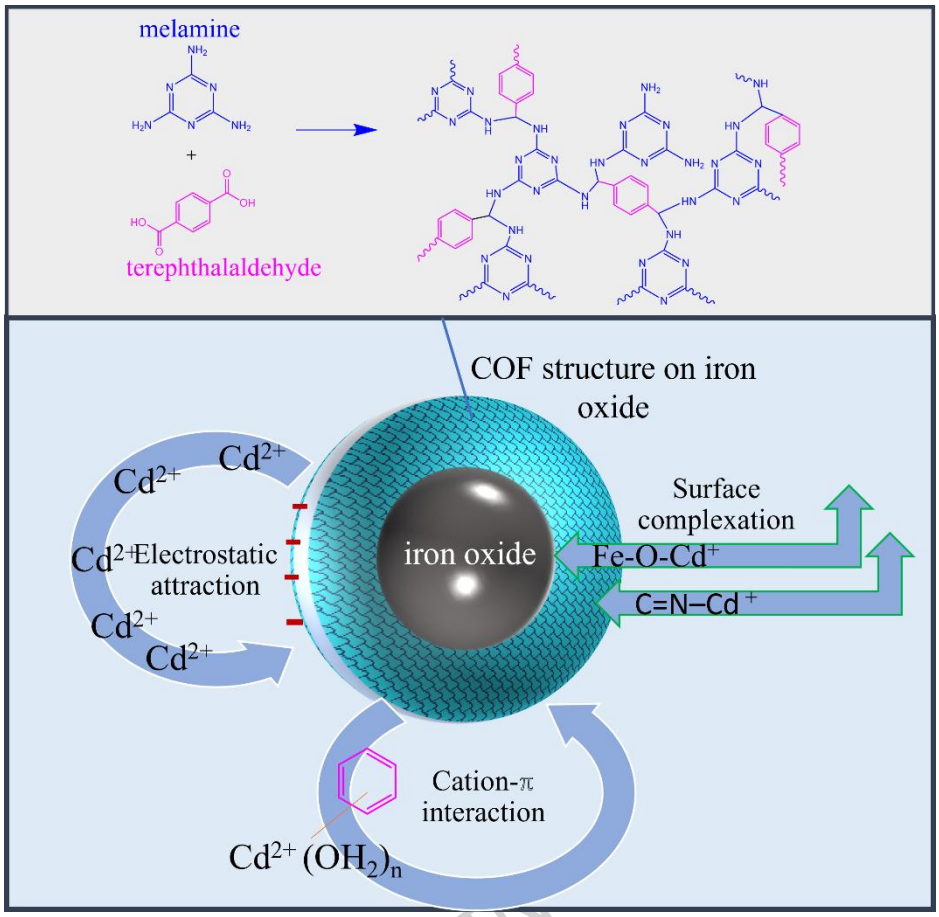


Fig 8. Possible adsorption mechanism of Cd^{2+} onto COF@Fe_3O_4 composite

Within this electrostatic setting, physical sorption may act as an initial enrichment step. The material presents nanoscale primary domains that assemble into secondary agglomerates, which likely provide a high effective area and short diffusion paths near the solid-liquid boundary. In line with this view, Weber-Morris analysis suggests an intraparticle diffusion contribution that assists transport into pores and interparticle regions, although diffusion does not appear to be the sole rate-limiting factor [59,63].

Once cadmium is enriched at the interface, chemical sorption could become predominant through inner-sphere complexation at deprotonated sites. Cd^{2+} may coordinate to surface -O-groups on magnetite to form Fe-O-Cd linkages, and to Lewis-basic nitrogen centers within the imine network of the COF shell [64]. The FT-IR features of the pristine composite (C=N and C-N bands together with Fe-O vibrations) are consistent with the availability of such donor environments, and kinetic fits that favor the pseudo-second-order model support a chemisorption-controlled step under the tested conditions. Post-use FT-IR spectra (Figure 9) show increased %T at about 3386, 1538 and 567 cm^{-1} relative to initial spectrum of material before adsorption (≈53.9%T at 1538 cm^{-1} and 61.5%T at 567 cm^{-1}), with partial recovery

ARTICLE IN PRESS

after regeneration, which is consistent with engagement of -OH and imine-adjacent nitrogen sites and with perturbation of Fe-O environments during Cd^{2+} binding and release.

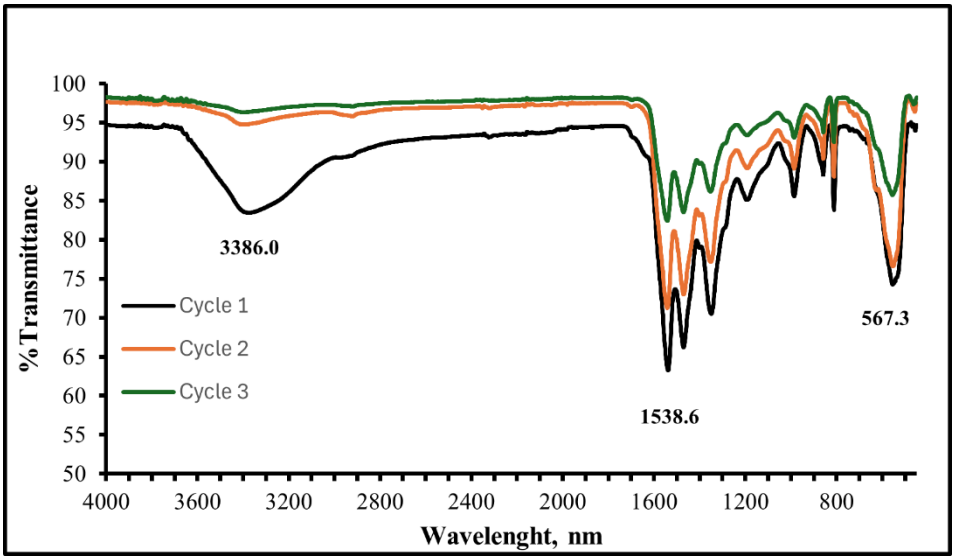


Fig. 9 Reusability FT-IR spectra for COF@Fe_3O_4 composite.

Ion exchange may operate as a specific manifestation of this chemical interaction. At hydroxylated surface sites, protons could be displaced by Cd^{2+} according to the reaction:

$$Fe\text{-}OH\ (surface) + Cd^{2+} \rightleftharpoons Fe\text{-}O\text{-}Cd^{+}\ (surface) + H^{+}$$

with local charge compensation by counter-ions from the medium. An analogous process can be envisaged at protonated nitrogen sites of the COF shell, which may be represented by:

$$\equiv C{=}N\text{-}H^{+}\ (surface) + Cd^{2+} \rightleftharpoons \equiv C{=}N\text{-}Cd^{+}\ (surface) + H^{+}$$

and reflects coordination of Cd^{2+} to imine-adjacent nitrogen accompanied by proton release. The increasing favorability of these reactions at higher pH aligns with the monotonic rise in removal and the dose study where additional sorbent increases the population of accessible donor sites until dissolved Cd^{2+} becomes limiting [65].

Taken together, the mechanism illustrated in Figure 8 is plausibly described as electrostatically guided access, followed by physical enrichment and chemically anchored fixation via inner-sphere complexation and proton-metal exchange, with diffusion assisting mass transfer but not acting as the sole kinetic limitation. This integrated interpretation coherently explains the pH dependence, the kinetic signature indicative of chemical sorption supported by diffusion, and the observed response to sorbent dose.

ARTICLE IN PRESS

3.6.Reusability and stability studies

In the reusability and stability study, a high Cd^{2+} concentration (100 mg L^{-1}), at the upper end of the concentration range used for estimating q_m, was employed so that changes in performance over cycles could be observed clearly. Reusability was evaluated using only magnetic recovery, water washing, and redrying between cycles. As displayed in Figure 10, removal efficiency was 68.88% in the first use, 63.51% in the second use, and 53.74% in the third use. This corresponds to a drop of 7.8% after one reuse and 22% after two reuses, . with good repeatability across replicates. The gradual decrease is compatible with partial persistence of chemically sorbed Cd^{2+} at deprotonated -OH and imine-adjacent sites that water alone does not fully reverse, together with minor contributions from physical factors such as aggregation or small material losses during handling. FT-IR profiles collected after each cycle, shown in Figure 10, display attenuation of O-H/N-H, C-N, and Fe-O bands after use with partial recovery after washing. The preservation of these characteristic bands across cycles indicates that the COF shell and Fe_3O_4 core remain structurally intact, and only a fraction of the donor groups becomes progressively less available due to stronger binding or incomplete desorption. This pattern aligns with a mixture of reversible physical or electrostatic association and more robust inner-sphere interactions. Importantly, all results were obtained without any acid or chelating regenerant, so water-only rinsing under mild conditions should be regarded as providing partial capacity recovery while also demonstrating the chemical and structural stability of the material over several cycles, rather than complete regeneration.

ARTICLE IN PRESS

ARTICLE IN PRESS

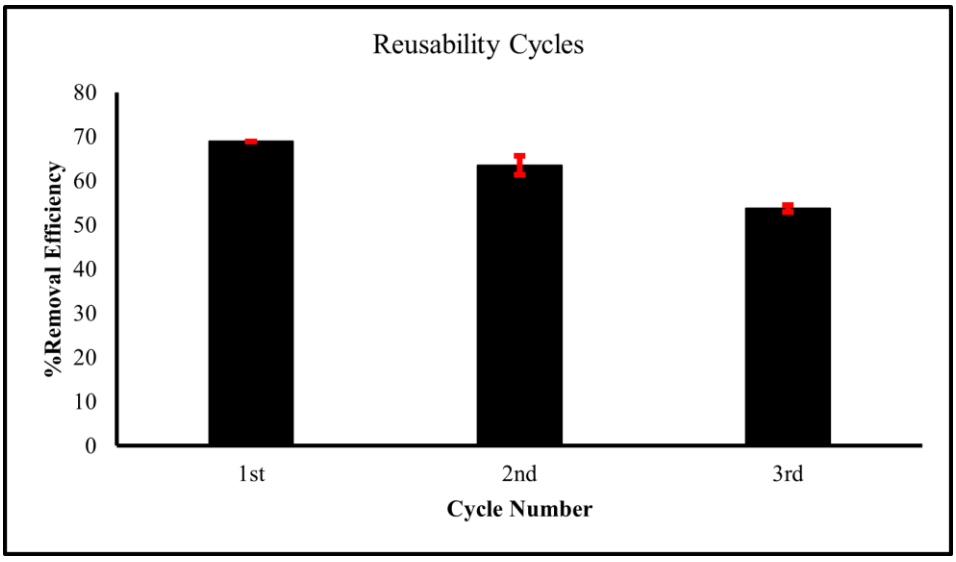


Fig 10. The reusability graph for Cd^{2+} removal with COF@Fe_3O_4 composites. Constant parameters: temp 298 K, concentration of Cd^{2+} (100 mg L^{-1}), pH 9.0 buffer, 30 min of mechanical shaker mixing, 50 mg adsorbent, agitation speed of 250 rpm.

3.7.Comparison with reported adsorbents

The COF@Fe_3O_4 composite developed in this study was evaluated through a comprehensive comparison with recent literature reports on Cd^{2+} adsorbents, including both COF-based and magnetically modified materials. While the adsorption capacity of COF@Fe_3O_4 (86-94 mg/g) is lower compared to some high-capacity COFs synthesized under idealized conditions, it performed effectively under realistic conditions, reaching near-complete Cd^{2+} removal from lake water using only magnetic separation. Key performance metrics are summarized in Table 5 to facilitate side-by-side comparison. For instance, β-ketoenamine COFs like TPE-catechol COF show good water stability and deliver slightly higher uptake (116 mg/g), but they depend on oxygen donor sites and tend to require tighter pH control [66]. Nitrogen-rich COFs without magnetic properties, such as triazine-linked frameworks, report very high capacities in idealized media up to 390 mg/g but their performance drops in complex waters with competing ions [67,68]. Porphyrin COFs immobilized on polyurethane supports are easier to handle and respond quickly, though they often suffer from reduced surface accessibility and slower diffusion [69]. Rice husk biochar-COF composites formed on biochar offer a lower-cost alternative, but their uptake is modest (58.6 mg/g), and they lack magnetic recovery or reuse testing [70]. Meanwhile, Fe_3O_4-EDTA nanocomposites combine wide pH usability and rapid adsorption, though they rely on acid regeneration and raise questions about long-term stability

ARTICLE IN PRESS

[71]. Taking these points into account, COF@Fe_3O_4 offers a practical mix of consistent performance, ease of handling, and reusability under environmentally relevant conditions.

Table 5. Comparative performance of COF-Based and magnetic adsorbents for Cd^{2+} removal

Adsorbent (Type)	Cd^{2+} Adsorption Capacity *(Langmuir q_{max})*	Optimal pH (Medium)	Equilibrium Time	Recovery Method	Reference
β-Ketoenamine COF *TPE-catechol COF*	116 mg/g	7 (stable pH 3-10; lab water)	Few hours	Filtration	[66]
N-Rich Functional COF *(triazine-linked COF beads)*	396 mg/g (DI water);156 mg/g (field water)	5-6 (DI lab solution)	Few hours	Filtration	[67,68]
Macroscale COF Composite - *Porphyrin COF on PU sponge*	~ 124 mg/g - 166 mg/g	8 (tap water.)	<1 h	Filtration	[69]
Magnetic Fe_3O_4-EDTA *Nano sorbent*	79.4 mg/g	3-10 (broad; simulated water)	<2 h	Magnetic	[71]
RH-COF composite*	58.62 mg/g	4-8 (DI lab solution)	Not specified	Filtration	[70]
COF@Fe_3O_4 Composite ***(This study)***	86-94 mg/g	9 (mildly alkaline; lake water)	30 min	Magnetic	-

**Covalent Organic Framework-Modified Biochar*

ARTICLE IN PRESS

4. CONCLUSION

This study presents a magnetically retrievable COF@Fe_3O_4 sorbent and demonstrates effective cadmium removal from lake water through a coherent characterization-kinetics-equilibrium framework. A pH_{pzc} near 4.2 explains the steady performance gain from pH 5.0 to 9.0 where residual Cd approached the detection limit, and the dose study showed diminishing gains beyond 50 mg, which was adopted for comparisons across 20-100 mg L^{-1} to reflect site availability rather than simple mass effects. Time-dependent uptake was described most consistently by a pseudo second order model with q_e = 44 mg g^{-1} and R^2 = 0.960, while intraparticle diffusion showed a positive intercept that indicates a diffusion contribution without serving as the sole resistance. Equilibrium analysis using parallel nonlinear and linear treatments identified Langmuir as the most suitable model, with q_{max} = 86.99 mg g^{-1} from nonlinear fitting and q_{max} = 93.67 mg g^{-1} from the linear form, both exceeding the maximum

ARTICLE IN PRESS

experimental q_e over 20-100 mg L^{-1} and indicating that saturation was not reached, and Toth also fit well and reflected mild site-energy heterogeneity that trends toward Langmuir behaviour at moderate to high C_e. Mechanistic indicators from the pH trend, pHpzc, dose response, kinetics, and spectral evolution across reuse cycles are consistent with electrostatically guided access, physical sorption on high-area domains, and inner-sphere interactions at deprotonated hydroxyl and imine-adjacent nitrogen sites, with proton–metal exchange at Fe-OH as a plausible contributor, while reusability and structural stability was confirmed by magnetic recovery with water-only rinsing. Overall, COF@Fe_3O_4 delivers high removal efficiencies in lake water with robust Langmuir capacities and practical magnetic handling, supporting further development toward continuous-flow operation, gentle regeneration to extend service life, and targeted surface functionalization to enhance capacity and matrix tolerance.

ARTICLE IN PRESS

Funding

The authors would like to thank Yıldız Technical University Scientific Research Projects Coordination Unit for the project supported in Project Number: FBA-2024-6094

Conflict of interest: The authors declare no conflict of interest.

Ethical Approval: Not applicable.

Consent to Participate: Not applicable.

Consent to Publish: Not applicable.

Availability of data and materials: Data and materials will be available on reasonable request from the corresponding author.

Authors Contributions:

Elif Öztürk Er: Conceptualization; Investigation; Methodology; Supervision; Validation; Writing - review & editing.

Selim Gürsoy: Formal analysis; Investigation; Methodology; Validation; Visualization; Roles/Writing - original draft.

Sezgin Bakırdere: Conceptualization; Investigation; Methodology; Supervision; Validation; Writing - review & editing.

ARTICLE IN PRESS

REFERENCES

1. Gürsoy, S. *et al.* Investigation of cadmium removal using tin oxide nanoflowers through process optimization, isotherms and kinetics. *Sci Rep* 15, 1–15 (2025).
2. Singh, A. *et al.* An approach towards different techniques for detection of heavy metal ions and their removal from waste water. *J Environ Chem Eng* 12, 113032 (2024).
3. Qi, F. *et al.* Cadmium solubility and bioavailability in soils amended with acidic and neutral biochar. *Science of The Total Environment* 610–611, 1457–1466 (2018).
4. He, Y. *et al.* Cadmium Exposure in Aquatic Products and Health Risk Classification Assessment in Residents of Zhejiang, China. *Foods 2023, Vol. 12, Page 3094* 12, 3094 (2023).
5. Adams, W. *et al.* Bioavailability Assessment of Metals in Freshwater Environments: A Historical Review. *Environ Toxicol Chem* 39, 48 (2020).
6. Lee, J. W. *et al.* Review of Cadmium Bioaccumulation in Fish Exposed to Cadmium. *Toxics* 13, 7 (2024).
7. Koli, A. K. & Whitmore, R. Distribution pattern of cadmium in different types of shellfish species. *Environ Int* 12, 559–561 (1986).
8. Rasin, P. *et al.* Exposure to cadmium and its impacts on human health: A short review. *Journal of Hazardous Materials Advances* 17, 100608 (2025).
9. Kurniawan, T. A., Chan, G. Y. S., Lo, W. H. & Babel, S. Physico–chemical treatment techniques for wastewater laden with heavy metals. *Chemical Engineering Journal* 118, 83–98 (2006).
10. Zhao, M., Xu, Y., Zhang, C., Rong, H. & Zeng, G. New trends in removing heavy metals from wastewater. *Applied Microbiology and Biotechnology 2016 100:15* 100, 6509–6518 (2016).
11. Oladimeji, T. E. *et al.* Review on the impact of heavy metals from industrial wastewater effluent and removal technologies. *Heliyon* 10, e40370 (2024).
12. Al-Zawahreh, K. A screening guide for efficient dye adsorbents under continuous flow conditions: a review. *Chemical Papers 2024 78:17* 78, 8919–8939 (2024).
13. Lange, K., Österlund, H., Viklander, M. & Blecken, G. T. Metal speciation in stormwater bioretention: Removal of particulate, colloidal and truly dissolved metals. *Science of The Total Environment* 724, 138121 (2020).
14. Al-Zawahreh, K. Guidelines for selecting efficient lead ion adsorbents: an overview. *Chemical Papers 2025 79:10* 79, 6445–6462 (2025).
15. Assefa, H. *et al.* Advances in adsorption technologies for hexavalent chromium removal: Mechanisms, materials, and optimization strategies. *Desalination Water Treat* 319, 100576 (2024).

ARTICLE IN PRESS

ARTICLE IN PRESS

16. Song, Y. & Ma, S. Pore engineering in metal–organic frameworks and covalent organic frameworks: strategies and applications. *Chem Sci* 16, 11740–11767 (2025).

17. da Silva, V. D. *et al.* Covalent organic frameworks as promising materials for the removal of metal and organic pollutants from water. *Materials Today Sustainability* 21, 100279 (2023).

18. Akhzari, S., Raissi, H. & Ghahari, A. Architectural design of 2D covalent organic frameworks (COFs) for pharmaceutical pollutant removal. *NPJ Clean Water* 7, 1–15 (2024).

19. Alamgir *et al.* Unlocking the potential of Metal-Organic frameworks for superior metal ions removal in wastewater treatment. *Inorg Chem Commun* 178, 114613 (2025).

20. Patial, S. *et al.* Rational design, structure properties, and synthesis strategies of dual-pore covalent organic frameworks (COFs) for potent applications: A review. *Environ Res* 218, 114982 (2023).

21. Liu, X. *et al.* Orderly Porous Covalent Organic Frameworks-based Materials: Superior Adsorbents for Pollutants Removal from Aqueous Solutions. *The Innovation* 2, 100076 (2021).

22. Mei, D. & Yan, B. Defect engineering in β-ketoenamine-linked covalent organic frameworks for high-efficiency uranium extraction. *J Mater Chem A Mater* 13, 14928–14939 (2025).

23. Xiong, K. *et al.* Tailoring β-ketoenamine covalent organic framework with azo for blue light-driven selective oxidation of amines with oxygen. *J Colloid Interface Sci* 665, 252–262 (2024).

24. Liu, X.-M., Su, Y.-T., Guo, J.-Z. & Li, B. Highly efficient Cr(VI) removal by cationic covalent organic framework.

25. Khosravani, M., Dehghani Ghanatghestani, M., Moeinpour, F. & Parvaresh, H. New sulfonated covalent organic framework for highly effective As(III) removal from water. *Heliyon* 10, e25423 (2024).

26. Abdelhamid, H. N., Sultan, S. & Mathew, A. P. Three-Dimensional Printing of Cellulose/Covalent Organic Frameworks (CelloCOFs) for CO2 Adsorption and Water Treatment. *ACS Appl Mater Interfaces* 15, 59795–59805 (2023).

27. Liu, L. Z. *et al.* Covalent organic framework-sodium alginate-Ca2+-polyacrylic acid composite beads for convenient dispersive solid-phase extraction of neonicotinoid insecticides in fruit and vegetables. *Food Chem* 441, (2024).

28. Liu, X. *et al.* Binder-free 3D printing of covalent organic framework (COF) monoliths for CO2 adsorption. *Chemical Engineering Journal* 403, 126333 (2021).

ARTICLE IN PRESS

ARTICLE IN PRESS

29. Schwab, M. G. *et al.* Catalyst-free preparation of melamine-based microporous polymer networks through Schiff base chemistry. *J Am Chem Soc* 131, 7216–7217 (2009).

30. Chen, S. *et al.* Imparting Ion Selectivity to Covalent Organic Framework Membranes Using de Novo Assembly for Blue Energy Harvesting Therefore, we propose a proof-of-concept synthesis of dye-encapsulated COF membranes through an interface-driven. *J. Am. Chem. Soc* 143, 39 (2021).

31. Uribe-Romo, F. J. *et al.* A Crystalline Imine-Linked 3-D Porous Covalent Organic Framework. *J. Am. Chem. Soc* 4570–4571 (2009) doi:10.1021/ja8096256.

32. Baun, A. *et al.* Rigidification of Poly(p-phenylene)s through ortho-Phenyl Substitution. *Macromolecules* 53, 5756–5762 (2020).

33. Hou, Y. *et al.* Enhanced Adsorption of Cadmium by a Covalent Organic Framework-Modified Biochar in Aqueous Solution. *Toxics* 12, 717 (2024).

34. Jiang, L. *et al.* Contributions of Various Cd(II) Adsorption Mechanisms by Phragmites australis-Activated Carbon Modified with Mannitol. *ACS Omega* 7, 10502–10515 (2022).

35. Yang, J., Huang, L., You, J. & Yamauchi, Y. Magnetic Covalent Organic Framework Composites for Wastewater Remediation. *Small* 19, 2301044 (2023).

36. Zhang, H. *et al.* Fe 3 O 4 @SiO 2-BD-DADB-COF is proposed as a novel magnetic covalent organic framework for the determination and extraction of 15 macrolide antibiotics in water and honey †. https://doi.org/10.1039/d5ra00080g (2025) doi:10.1039/d5ra00080g.

37. Guillem-Navajas, A. *et al.* Iron Oxyhydroxide-Covalent Organic Framework Nanocomposite for Efficient As(III) Removal in Water. *ACS Appl Mater Interfaces* 14, 50163–50170 (2022).

38. Gürsoy, S., Zeytinci, N. K., Zaman, B. T., Bakırdere, S. & Öztürk Er, E. Study of linear and nonlinear isotherm and kinetic parameters of hexavalent chromium adsorption onto reduced graphene oxide coated iron oxide. *Sci Rep* 15, 1–17 (2025).

39. You, L. *et al.* Facile synthesis of Fe3O4@COF covalent organic frameworks for the adsorption of bisphenols from aqueous solution. *J Mol Liq* 320, 114456 (2020).

40. Koşal Şahin, S. & Taş Divrik, M. Evaluation of the Aquatic Oligochatea Fauna and Seasonal Changes in Water Quality of the Büyükçekmece Dam Lake, which Provides Water to İstanbul. *Journal of Limnology and Freshwater Fisheries Research* 10, 126–133 (2024).

41. Brdar, M., Šćiban, M., Takači, A. & Došenović, T. Comparison of two and three parameters adsorption isotherm for Cr(VI) onto Kraft lignin. *Chemical Engineering Journal* 183, 108–111 (2012).

ARTICLE IN PRESS

ARTICLE IN PRESS

42. Wang, J., Guo, X., Tsang, D. & Ma, L. Q. Adsorption kinetics and isotherm models of heavy metals by various adsorbents: An overview. *Crit Rev Environ Sci Technol* 53, 1837–1865 (2023).

43. Mahanty, B., Behera, S. K. & Sahoo, N. K. Misinterpretation of Dubinin–Radushkevich isotherm and its implications on adsorption parameter estimates. *Separation Science and Technology (Philadelphia)* 58, 1275–1282 (2023).

44. Zhou, X., Maimaitiniyazi, R. & Wang, Y. Some consideration triggered by misquotation of Temkin model and the derivation of its correct form. *Arabian Journal of Chemistry* vol. 15 Preprint at https://doi.org/10.1016/j.arabjc.2022.104267 (2022).

45. Coates, J. Interpretation of Infrared Spectra, A Practical Approach. *Encyclopedia of Analytical Chemistry* https://doi.org/10.1002/9780470027318.A5606 (2000) doi:10.1002/9780470027318.A5606.

46. Joseph, T. *et al.* Spectroscopic (FT-IR, FT-Raman), first order hyperpolarizability, NBO analysis, HOMO and LUMO analysis of N-[(4-(trifluoromethyl)phenyl]pyrazine-2-carboxamide by density functional methods. *Arabian Journal of Chemistry* 10, S2281–S2294 (2017).

47. Scaria, J., Gopinath, A. & Nidheesh, P. V. A versatile strategy to eliminate emerging contaminants from the aqueous environment: Heterogeneous Fenton process. *J Clean Prod* 278, 124014 (2021).

48. Guzman, K. A. D., Finnegan, M. P. & Banfield, J. F. Influence of Surface Potential on Aggregation and Transport of Titania Nanoparticles. *Environ Sci Technol* 40, 7688–7693 (2006).

49. Pérez-Ramírez, J., Christensen, C. H., Egeblad, K., Christensen, C. H. & Groen, J. C. Hierarchical zeolites: enhanced utilisation of microporous crystals in catalysis by advances in materials design. *Chem Soc Rev* 37, 2530–2542 (2008).

50. Appel, C. & Ma, L. Concentration, pH, and Surface Charge Effects on Cadmium and Lead Sorption in Three Tropical Soils. *J Environ Qual* 31, 581–589 (2002).

51. Hou, Y. *et al.* Enhanced Adsorption of Cadmium by a Covalent Organic Framework-Modified Biochar in Aqueous Solution. *Toxics* 12, 717 (2024).

52. da Silva Alves, D. C., Healy, B., Pinto, L. A. de A., Cadaval, T. R. S. & Breslin, C. B. Recent Developments in Chitosan-Based Adsorbents for the Removal of Pollutants from Aqueous Environments. *Molecules 2021, Vol. 26, Page 594* 26, 594 (2021).

53. Boruah, H., Tyagi, N., Gupta, S. K., Chabukdhara, M. & Malik, T. Understanding the adsorption of iron oxide nanomaterials in magnetite and bimetallic form for the removal of arsenic from water. *Front Environ Sci* 11, 1104320 (2023).

54. Pang, Y. *et al.* Cadmium adsorption performance and mechanism from aqueous solution using red mud modified with amorphous MnO2. *Sci Rep* 12, 4424 (2022).

ARTICLE IN PRESS

ARTICLE IN PRESS

55. Hegazy, G. E., Soliman, N. A., Ossman, M. E., Abdel-Fattah, Y. R. & Moawad, M. N. Isotherm and kinetic studies of cadmium biosorption and its adsorption behaviour in multi-metals solution using dead and immobilized archaeal cells. *Sci Rep* 13, 2550 (2023).

56. Li, X. *et al.* Adsorption of Cd (II) by a novel living and non-living Cupriavidus necator GX_5: optimization, equilibrium and kinetic studies. *BMC Chem* 17, 54 (2023).

57. Tafakori, V., Zadmard, R., Tabandeh, F., Amoozegar, M. A. & Ahmadian, G. Equilibrium Isotherm, Kinetic Modeling, Optimization, and Characterization Studies of Cadmium Adsorption by Surface-Engineered Escherichia coli. *Iran Biomed J* 21, 380 (2017).

58. Simonin, J. P. On the comparison of pseudo-first order and pseudo-second order rate laws in the modeling of adsorption kinetics. *Chemical Engineering Journal* 300, 254–263 (2016).

59. Dharmarathna, S. P. & Priyantha, N. Investigation of boundary layer effect of intra-particle diffusion on methylene blue adsorption on activated carbon. *Energy Nexus* 14, 100294 (2024).

60. Batool, F., Akbar, J., Iqbal, S., Noreen, S. & Bukhari, S. N. A. Study of Isothermal, Kinetic, and Thermodynamic Parameters for Adsorption of Cadmium: An Overview of Linear and Nonlinear Approach and Error Analysis. *Bioinorg Chem Appl* 2018, 3463724 (2018).

61. Daou, T. J. *et al.* Phosphate Adsorption Properties of Magnetite-Based Nanoparticles. *Chemistry of Materials* 19, 4494–4505 (2007).

62. Yang, J. *et al.* Protonated Imine-Linked Covalent Organic Frameworks for Photocatalytic Hydrogen Evolution. *Angew Chem Int Ed Engl* 60, 19797 (2021).

63. Wang, J. & Guo, X. Rethinking of the intraparticle diffusion adsorption kinetics model: Interpretation, solving methods and applications. *Chemosphere* 309, 136732 (2022).

64. Wu, S. *et al.* Cadmium Immobilization on Fe Oxyhydroxides Enhanced by DOM Using Single-Molecule Determinations. *Environ Sci Technol* 59, 3771–3779 (2025).

65. Randall, S. R., Sherman, D. M., Ragnarsdottir, K. V. & Collins, C. R. The mechanism of cadmium surface complexation on iron oxyhydroxide minerals. *Geochim Cosmochim Acta* 63, 2971–2987 (1999).

66. Liu, N. *et al.* A heteropore covalent organic framework for adsorptive removal of Cd(II) from aqueous solutions with high efficiency. *Chinese Chemical Letters* 31, 386–390 (2020).

67. Gatou, M. A., Bika, P., Stergiopoulos, T., Dallas, P. & Pavlatou, E. A. Recent Advances in Covalent Organic Frameworks for Heavy Metal Removal Applications. *Energies (Basel)* 14, (2021).

ARTICLE IN PRESS

ARTICLE IN PRESS

68. Bhunia, P., Chatterjee, S., Rudra, P. & De, S. Chelating polyacrylonitrile beads for removal of lead and cadmium from wastewater. *Sep Purif Technol* 193, 202–213 (2018).

69. Jin, W. L. *et al.* Sponge-supported monolithic materials of porphyrin covalent organic frameworks for selective recognition, convenient removal and extraction of Cd2+. *J Environ Chem Eng* 10, (2022).

70. Hou, Y. *et al.* Enhanced Adsorption of Cadmium by a Covalent Organic Framework-Modified Biochar in Aqueous Solution. *Toxics* 12, (2024).

71. Huang, Y. & Keller, A. A. EDTA functionalized magnetic nanoparticle sorbents for cadmium and lead contaminated water treatment. *Water Res* 80, 159–168 (2015).

ARTICLE IN PRESS